Available online at www.sciencedirect.com
SCIENCE DIRECT
International Journal of Heat and Mass Transfer 49 (2006) 4567–4576
International Journal of HEAT and MASS TRANSFER
www.elsevier.com/locate/ijhmt

Numerical simulation of thermocapillary nonwetting

J.-C. Chen [a,*], C.-W. Kuo [a], G.P. Neitzel [b]

[a] Department of Mechanical Engineering, National Central University, Chung-Li 320, Taiwan, ROC
[b] George W. Woodruff School of Mechanical Engineering, Georgia Institute of Technology, Atlanta, GA 30332-0405, USA

Received 9 September 2005; received in revised form 22 March 2006
Available online 7 July 2006

Abstract

The nonwetting phenomenon that occurs when a liquid drop is pressed against a solid wall held at a sufficiently lower temperature, is analyzed numerically. An interstitial gas film, induced by thermocapillary convection, separates the drop from the wall, forming a self-lubricating system. The temperature differences and wall distances were probed to evaluate their nonwetting effect. The results indicate that increasing the temperature difference or decreasing the wall distance can enhance the wetting suppression, whether with silicone-oil or water. The thermocapillary nonwetting phenomenon using 5 cSt silicone-oil droplet is more apparent than that obtained with water when the wall distance is small enough, because the capillary number of silicone oil is much larger than that of water. Alternately, when a cold liquid drop is moved towards a hot wall, the thermocapillary flow encourages the occurrence of wetting.

Keywords: Noncoalescence; Nonwetting; Thermocapillary convection; Droplet; Free-surface deformation

1. Introduction

Recent experiments performed by Dell'Aversana et al. [1–3] have demonstrated that, in the presence of a surrounding gas, the coalescence of two bodies of the same fluid that come into apparent contact and the wetting of a solid surface pressed against a drop, can be prevented by controlling the temperature difference between them. This noncoalescence or nonwetting behavior is attributable to the existence of a lubricating gas film driven by surface motion that keeps the liquid–liquid or liquid–solid surfaces from coming into actual contact. The gas motion is driven by a thermocapillary-induced motion of the droplet free surface (which also drives flow within the droplets) that is generated by the existence of a temperature-induced surface-tension gradient along the gas–liquid interface. These instances have been referred to as "self-lubricated systems" and recent papers by Dell'Aversana and Neitzel [4] and Neitzel and Dell'Aversana [5] discuss these and other related phenomena.

If two such surfaces are pressed together with sufficient force, either the contact line that holds the liquid to the solid will fail, causing the liquid to spill out onto the surface, or the lubricating film will disappear, resulting in coalescence or, in the case of a liquid and solid, wetting.

The ability of the thermocapillary-driven lubricating gas film to withstand the load between the two opposing surfaces is a function of the temperature difference between the two noncontacting surfaces, the volume of the droplet, the relative distance between the two surfaces, and the physical properties of the liquid and the gas. Dell'Aversana et al. [1] show that, with a fixed load, two 5 cSt silicone-oil drops do not coalesce when the temperature difference between them exceeds a certain value and Dell'Aversana and Neitzel [3] have shown that noncoalescence can be maintained with very low static pressure in the surrounding gas. These temperature-difference and pressure thresholds vary with the fluid type; this thermocapillary-induced noncoalescence phenomenon has not yet been observed to occur with water.

* Corresponding author. Tel.: +886 3 426 7321; fax: +886 3 425 4501.
E-mail address: jcchen@cc.ncu.edu.tw (J.-C. Chen).

0017-9310/$ - see front matter © 2006 Elsevier Ltd. All rights reserved.
doi:10.1016/j.ijheatmasstransfer.2006.04.033

Nomenclature

Ca_l	capillary number, $\left(=\frac{\gamma_{l,T}\Delta T}{\gamma_l}\right)$
C_p	specific heat, J kg^{-1} °C^{-1}
D	distance between walls, m
H	mean curvature of surface, m^{-1}
i	unit vector in x-direction
j	unit vector in y-direction
k	thermal conductivity, W m^{-1} °C^{-1}
Kn	Knudsen number ($=\lambda/\delta$)
Ma_l	Marangoni number, $\left(=\frac{\gamma_{l,T}\Delta TR}{\alpha_l\mu_l}\right)$
n	normal vector of interface
P	pressure, Pa(=N m^{-2})
Pr	Prandtl number, $(=\frac{\nu}{\alpha})$
r	local free surface radius, mm
R	drop radius, m
S	gas–liquid interface, m
T	temperature, °C
u	velocity component in x-direction, m s^{-1}
v	velocity component in y-direction, m s^{-1}
V	velocity vector, m s^{-1}
V_s	resultant speed on the drop's free surface, m s^{-1}
x	coordinate, m
y	coordinate, m

Greek symbols

α	thermal diffusivity, m^2 s^{-1}
Δ	difference
δ	thickness of the lubricating film, m
Γ	drop volume, m^2
γ	surface tension, kg s^{-2}
$\gamma_{l,T}$	surface-tension/temperature coefficient
λ	mean free path of air, m
μ	dynamic viscosity, kg m^{-1} s^{-1}
ν	kinematic viscosity, m^2 s^{-1}
ρ	density of fluid, kg m^{-3}
σ	stress vector, kg m^{-1} s^{-2}

Subscripts

a	air
C	cold wall
H	hot wall
i	phase
l	liquid
n	normal direction
ref	reference state
s	silicone-oil
t	tangential direction
w	water

Dell'Aversana et al. [2] measured the shape of the liquid–gas interface of a drop pressed against a solid surface by means of laser interferometry. When the drop exhibits nonwetting behavior a dimple appears, which deepens and widens as the load increases; this has also been observed for cases of noncoalescence. The thickness of the interstitial gas film is of the order of a few microns for a 5×10^{-3} m diameter silicone-oil drop. Since it is very difficult to observe or measure the velocity and temperature fields inside this gas film, an appropriate theoretical treatment is needed to better understand the influence of the gas motion on these noncoalescence nonwetting phenomena.

Sumner et al. [6] have examined the liquid and gas flows in a two-dimensional nonwetting drop using lubrication theory, which is only suitable for an ideal slender drop with smaller thermocapillary convection. They find that the presence of a central dimple observed experimentally requires the inclusion of inertia to be present.

Simulations of a nonwetting droplet are complicated by the disparity of length scales involved. Typical droplet sizes are of O (mm) while film thicknesses are O (μm). Numerical simulations of thermocapillary-driven noncoalescence and nonwetting were performed by Monti et al. [7,8]. They neglected flow-induced free-surface deformation, calculating the flow in the surrounding gas. However, the shape of free surface was not updated using results from gas-flow calculations in conjunction with the normal-stress boundary condition. The present simulation computes flows in the liquid and gas phases simultaneously, adjusting the interface position through the use of the stress boundary conditions imposed thereon.

In the present study, the commercial code FIDAP based on finite element techniques has been employed to perform a numerical simulation of thermocapillary wetting suppression. FIDAP has proven useful for problems involving thermocapillary flow [9]. The physical problem considered here is a two-dimensional liquid drop attached to a support and pressed against a wall held at a different temperature. This case corresponds to that treated experimentally by Nalevanko [10] and examined theoretically using lubrication theory by Sumner et al. [6]. As mentioned above, the flow in both the gas and liquid phases must be computed simultaneously to simulate thermocapillary nonwetting. We explore the velocity and thermal fields within both the lubricating film and the liquid drop. A steady-state solution is also discussed, with many parameters being considered, i.e., the drop/wall temperature differences and rel-

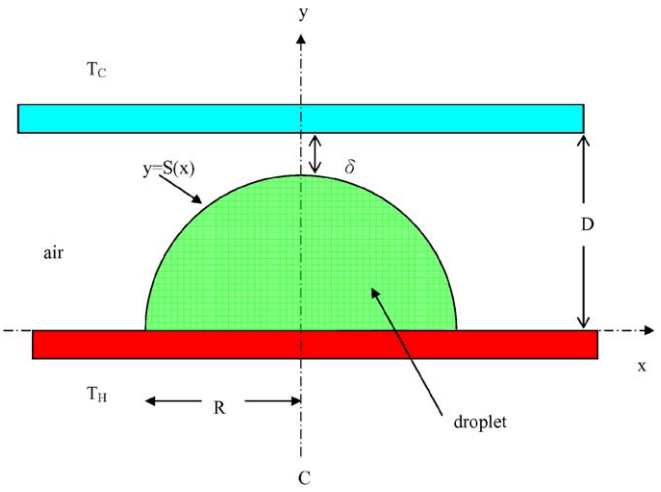

Fig. 1. Physical model of the simulation.

ative displacement from the point of first apparent contact, as well as considering two different drop liquids.

2. Mathematical formulation

A two-dimensional semicircular drop with a radius R is attached to a hot lower surface while the cold upper surface is pushed downward towards the liquid drop. Usually, the drops in the experiments [1,10] were formed by injecting liquid from a reservoir through a hole or slot in the pedestal to which the droplet is affixed. Therefore, the contact lines are assumed to be pinned at $x = \pm R$ on the lower surface. The two parallel solid surfaces are separated by a distance D, as shown in Fig. 1. The temperatures of the hot and the cold surfaces are T_H and T_C, respectively. The drop is an incompressible, Newtonian liquid surrounded by air. According to the estimate of Dell'Aversana et al. [2], the Knudsen number $Kn = \lambda/\delta$ is less than 10^{-2}, where λ is the mean free path of air and δ is the thickness of the lubricating film of air. A continuum model employing a no-slip boundary condition is thereby assumed to hold for the gas phase. The gas flow is also assumed to be incompressible in light of the air velocity. Because the temperature difference between the walls considered in the present study is not too large, constant fluid properties are assumed with the exception of the surface tension, which is assumed to vary linearly with the temperature as described below. The liquid volume of the drop is small, so gravity (buoyancy) may be safely neglected in these computations.

The governing equations for this model are the continuity, Navier–Stokes, and energy equations:

$$\nabla \cdot \mathbf{V}_i = 0, \tag{1}$$

$$\rho_i[(\mathbf{V}_i \cdot \nabla)]\mathbf{V}_i = -\nabla P_i + \mu_i \nabla^2 \mathbf{V}_i, \tag{2}$$

$$\rho_i C_{pi}(\mathbf{V}_i \cdot \nabla T_i) = k_i \nabla^2 T_i, \tag{3}$$

where $\mathbf{V}_i = u_i\mathbf{i} + v_i\mathbf{j}$ is the velocity vector, P_i is the pressure, T_i is the temperature, ρ_i is the density, μ_i is the dynamic viscosity, C_{pi} is the specific heat, and k_i is the thermal conductivity. The subscript "i" = "l" denotes the liquid phase ("l" = "s", if the liquid is silicone oil; "l" = "w", if the liquid is water) and "i" = "a" represents a gas.

The surface tension of a particular liquid γ_l is considered to be a linear function of the temperature, viz.,

$$\gamma_l = \gamma_{l,\mathrm{ref}} - \gamma_{l,T}(T_l - T_{\mathrm{ref}}), \tag{4}$$

where $\gamma_{l,\mathrm{ref}}$ is the surface tension at temperature $T_{\mathrm{ref}} = T_C$ and $\gamma_{l,T}$ is the surface-tension/temperature coefficient. The gas–liquid interface described by $y = S(x)$ satisfies the kinematic condition, appropriate shear- and normal-stress conditions, no-slip and continuity of temperature at the interface:

$$\mathbf{V}_l \cdot \nabla S = \mathbf{V}_a \cdot \nabla S, \tag{5}$$

$$\boldsymbol{\sigma}_l - \boldsymbol{\sigma}_a = 2\gamma_l H n - \nabla\gamma_l, \tag{6}$$

$$\mathbf{V}_l = \mathbf{V}_a, \tag{7}$$

$$T_l = T_a, \tag{8}$$

where H is the mean curvature of the surface, n is the normal vector of interface, and $\boldsymbol{\sigma}_i$ is the stress vector. Continuity of heat flux at the interface is satisfied as a natural boundary condition with the finite-element technique employed for solution. The droplet's volume is conserved, requiring

$$\int_{-R}^{R} S(x)\mathrm{d}x = \Gamma, \tag{9}$$

where Γ is the drop volume per unit length. The boundary conditions on the hot and cold surfaces are described below:

$$u_a = v_a = 0,\ T = T_C \quad \text{for } y = D \quad \text{and} \quad -\infty \leqslant x \leqslant \infty, \tag{10}$$

$$u_i = v_i = 0,\ T = T_H \quad \text{for } y = 0 \quad \text{and} \quad -R \leqslant x \leqslant R, \tag{11}$$

$$\frac{\partial u_a}{\partial x} = \frac{\partial v_a}{\partial y} = \frac{\partial T}{\partial x} = 0 \quad \text{for } |x| \to \infty \quad \text{and} \quad 0 \leqslant y \leqslant D. \tag{12}$$

Finally, the pinning condition at $x = \pm R$ requires that

$$S(-R) = S(R) = 0. \tag{13}$$

From the previous experimental results [2], the interstitial film thickness is about O (μm). Therefore, using a numerical simulation to investigate the present thermocapillary nonwetting problem involves three difficulties: dissimilar length scales associated with droplet and interstitial film, moving gas–liquid interface, and couple effect of gas and liquid flow fields. FIDAP has been used successfully to compute the moving gas–liquid interface problem without considering the effect from the gas field. In the present approach, we extend FIDAP code to simulate the thermocapillary nonwetting problem incorporating the existence of gas flow motion. The physical domain seen in Fig. 1 was subdivided into elements, which form a grid. The complex geometrics can be handled with unstructured quadrilateral simplex elements. The total number of elements in the whole continuum field, including both drop and air, was 3310. Different numbers of finite elements

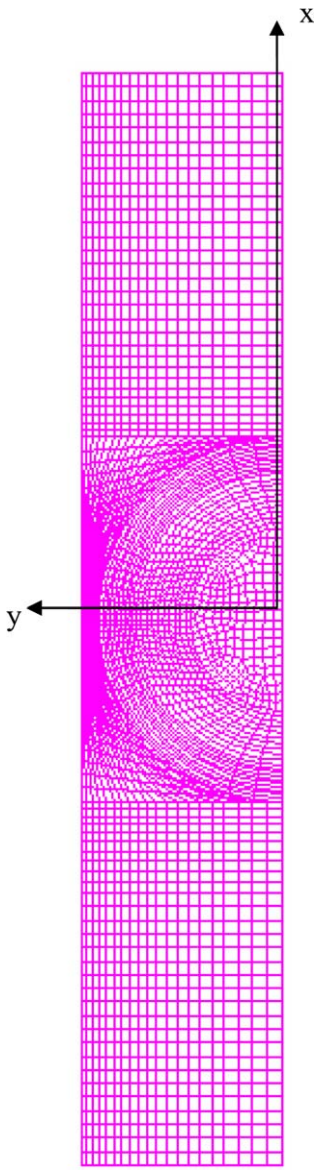

Fig. 2. Mesh configuration of the physical domain.

were examined, and the use of 3310 elements demonstrated the best combination of accuracy and computation time. To solve the difficulty of disparate length scales associated with droplet and interstitial film, an appropriate finer mesh is applied near the free surface in both liquid and gas fields, as shown in Fig. 2; the nodes on the free surface are permitted to move in the direction of the local normal. The above partial-differential equations and boundary conditions were discretized using the Galerkin finite-element method (GFEM) and the resulting nonlinear algebraic equations were then solved using the uncoupled (i.e., segregated-solver) method. Each degree of freedom was solved separately. The associated flow problem was solved while the appropriate boundary condition was fixed; iterations were continued until velocity convergence to within a preset tolerance (less than 10^{-6}) was satisfied. The location of the free surface was updated using the normal-stress balance. This procedure was repeated until the position of the free surface converged. A combination of relaxing the pressure and the use of an upwinding scheme was introduced to prevent unphysical wiggles in the flow solution.

The simulation methodology developed by the present approach based on the FIDAP has been used to compute the isothermal wetting suppression case in the presence of shear when a drop approaches a moving wall [13]. Smith and Neitzel [14] develop a hybrid numerical model employing lubrication theory for the interstitial film and numerical simulation for the liquid and outer gas fields. The deficiency of their model is that the net flow rate of gas field must provide artificially. On the contrary, the present model is without this limitation. With the same physical conditions, those from the two models agree quite well.

3. Results and discussion

Simulations were performed to investigate the surface deformation of a semicircular drop immersed in air with an initial radius of $R = 1 \times 10^{-3}$ m. The influences of the temperature difference ΔT and the distance D between the two parallel walls were determined. The liquids considered were 5 cSt silicone-oil and water; their physical properties are listed in Table 1.

The thermocapillary nonwetting experiments [2] have been conducted by imposing a constant temperature difference of 35 °C between a droplet attached to a heated rod pressed against a cooled glass surface. The temperature difference cannot be too large (which depends on the volatility of the liquid employed) to minimize evaporation of liquid from the droplet. With the experiments in mind, the temperature difference between hot and cold walls is selected for the present computations to be $\Delta T = 10$, 30, and 50 °C. The numerical computation exhibited problems with convergence of the solution when the distance between two walls is less than 1.01×10^{-3} m. The experimental results [2] also reveal that the interstitial film thickness measured by interferometry is O (μm). Hence, the distance between two walls is chosen for the computations to be $D = 1.01 \times 10^{-3}$, 1.03×10^{-3}, and 1.05×10^{-3} m.

Table 1
Fluid material properties

	ρ (kg m^{-3})	γ (kg s^{-2}) @ 20 °C	$\gamma_{l,T}$ (kg s^{-2} °C^{-1})	μ (kg m^{-1} s^{-1})	α (m^2 s^{-1})
Silicone oil	9.1×10^2	1.92×10^{-2}	6.893×10^5	4.55×10^3	6.15×10^{-8}
Water	9.98×10^2	7.27×10^{-2}	1.6×10^4	1.002×10^3	1.42×10^{-7}
Air	1.21			1.528×10^5	2.216×10^{-5}

Fig. 3 displays the streamlines and isotherms for silicone oil when $T_C = 20$ °C, $\Delta T = 30$ °C and $D = 1.01 \times 10^{-3}$ m. A pair of symmetric, counter-rotating vortices, generated by temperature-induced surface-tension gradients, appears inside the droplet. The silicone oil near the liquid–gas interface moves from hot to cold locations, flowing back along symmetrical lines extending from the vertex to the base of the drop that is attached to the hot wall. The thermocapillary movement causes not only bulk motion of the liquid inside the drop, but also bulk flow within the air surrounding it. The air near the liquid–gas interface is swept by the motion of the silicone oil into the small gap and flows out along the cold wall to form the lubricating film, and this bulk flow generates a pair of symmetric, counter-rotating vortices in the ambient air surrounding the drop.

The Prandtl number ($Pr = \frac{\nu}{\alpha}$, where α is the thermal diffusivity and ν is the kinematic viscosity) characterizes the relative importance of convective and diffusive thermal transport. The Prandtl number ($Pr_s = 74$) for 5 cSt silicone-oil is very large. Thus, the isotherms indicate the heat transport to have been strongly influenced by convection; the isotherm pattern in the drop indicates that it is well-mixed. Computations by Carpenter and Homsy [11] of 2-D buoyant-thermocapillary flow in a rectangular geometry showed this same, well-mixed core when thermocapillarity dominates buoyancy. The largest temperature gradients appear near the hot and the cold walls.

Fig. 4 shows the temperature, resultant velocity ($V_s = \sqrt{u^2 + v^2}$), and pressure difference ($\Delta P = P_a - P_l$) distributions on the silicone-oil drop's free surface, when $T_C = 20$ °C and $D = 1.01 \times 10^{-3}$ m, with $\Delta T = 10$, 30, and 50 °C. Evidence of enhanced thermocapillary convection for increasing ΔT can be observed by comparing the curves in Fig. 4(a). The solutions exhibit larger temperature variations near the cold wall ($x = 0$) and the hot wall ($x = 1$), whereas the temperature gradients far from both

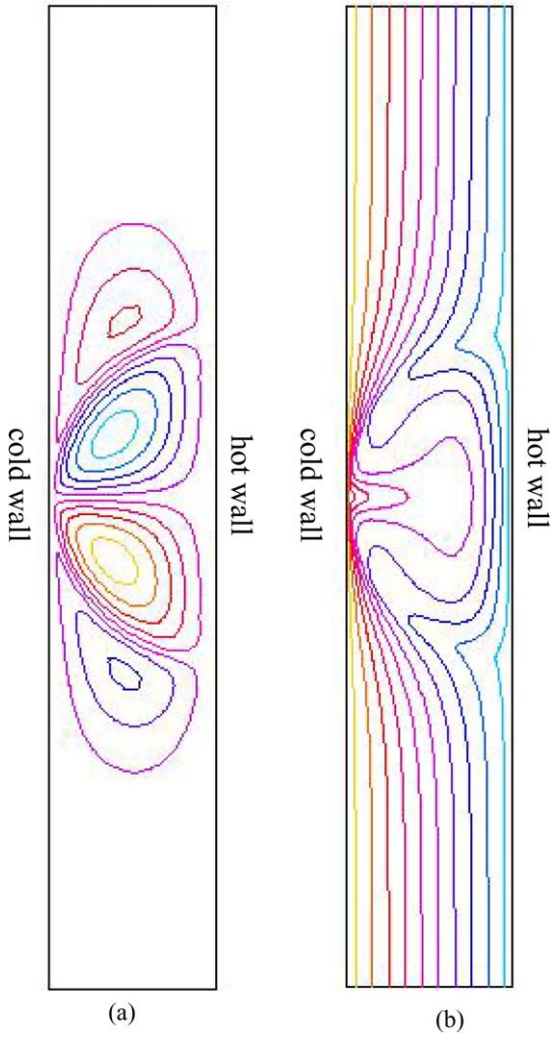

Fig. 3. (a) Streamline contours and (b) isotherms for a hot drop pressed against a cold wall held at $T_C = 20$ °C, when $\Delta T = 30$ °C and $D = 1.01 \times 10^{-3}$ m.

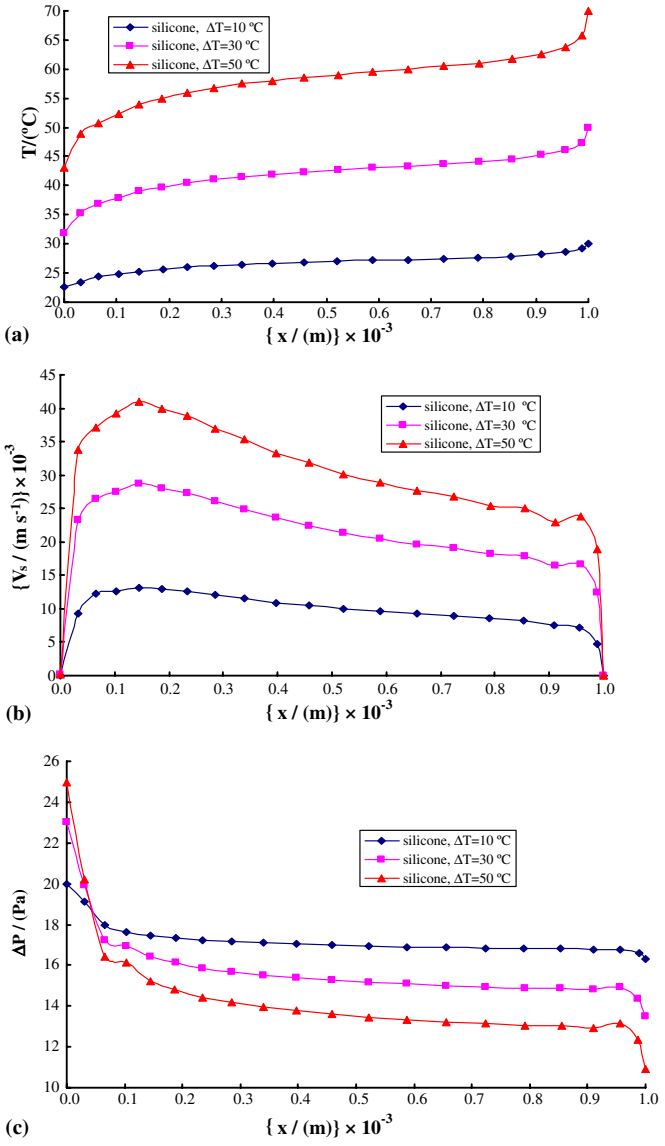

Fig. 4. (a) Temperature, (b) resultant velocity, (c) pressure difference versus x, for a silicone-oil drop with $D = 1.01 \times 10^{-3}$ m and three different ΔT.

walls is smaller, especially for a larger ΔT. The magnitude of the resultant free-surface velocity (Fig. 4(b)) is zero at the contact lines $(x, y) = (\pm 1, 0)$, as required by boundary condition (11), while another zero-velocity point appears at the stagnation point $(x, y) = (0, S(0))$, where the maximum pressure difference is observed (Fig. 4(c)). The velocity increases significantly when ΔT is increased, indicating the dynamic pressure is higher for a larger ΔT. The pressure difference increases dramatically when the stagnation point is approached because the static pressure increases as the dynamic pressure decreases. Therefore, as ΔT becomes large, the pressure difference near the stagnation point increases. The pressure difference for the position away from the stagnation point is smaller for higher ΔT, since it possesses a higher dynamic pressure.

The temperature, resultant velocity, and pressure difference distributions on a water free surface are shown in Fig. 5, where $T_C = 20\ ^\circ\mathrm{C}$ and $D = 1.01 \times 10^{-3}$ m, with $\Delta T = 10$, 30, and 50 °C. The trend for the temperature distribution of water (Fig. 5(a)) is similar to that of silicone oil (Fig. 4(a)). Near the cold wall, the corresponding free-surface temperature of water is higher than that of silicone oil, i.e., a more significant temperature drop-off exists in the lubricating film for water, for the same ΔT, as can be seen by comparing the curves in Figs. 4 and 5(a). The Marangoni number for this situation is defined as $Ma_l = \frac{\gamma_{l,T}\Delta TR}{\alpha_l \mu_l}$ [12], a larger Marangoni number indicative of stronger thermocapillary convection. At $\Delta T = 30\ ^\circ\mathrm{C}$, the Marangoni number of water $\left(Ma_w = \frac{\gamma_{w,T}\Delta TR}{\alpha_w \mu_w} = 50\,600\right)$ is much larger than that of silicone oil $\left(Ma_s = \frac{\gamma_{s,T}\Delta TR}{\alpha_s \mu_s} = 10\,064\right)$. Therefore, the thermocapillary convection inside a water drop is more vigorous than that inside a silicone-oil drop experiencing the same ΔT. Hence, the free-surface velocity of water (Fig. 5(b)) is much larger than the corresponding one for silicone-oil (Fig. 4(b)). In turn, this makes the pressure difference for water (Fig. 5(c)) greater than that for silicone-oil (Fig. 4(c)).

We also investigate the effect of the distance between the cold wall and the vertex of a hot drop. Fig. 6 shows the influence of different distances ($D = 1.01 \times 10^{-3}$, 1.03×10^{-3}, and 1.05×10^{-3} m) for a silicone-oil drop with $\Delta T = 30\ ^\circ\mathrm{C}$. The thermal resistance of the interstitial film will decrease as its thickness decreases. This explains why the temperature gradients are enlarged for a smaller D, as observed in Fig. 6(a). Obviously, decreasing D can enhance the strength of the thermocapillary flow by increasing the surface-temperature gradients near the drop vertex and contact lines. As D decreases, the velocities along the free surface are larger (Fig. 6(b)), while the pressure difference varies accordingly (Fig. 6(c)). The trends for water drops are similar to those for silicone-oil drops.

The distance $r(x)$ from the origin to a point on the free surface is plotted as a function of x in Fig. 7(a), indicating that the silicone-oil drop forms a dimple at the stagnation point, resulting in a bulge away from this point. These phenomena become more notable as ΔT increases, for $D = 1.01 \times 10^{-3}$ m and $\Delta T = 10$, 30, and 50 °C. The capillary number, defined as $Ca_l = \frac{\gamma_{l,T}\Delta T}{\gamma_l}$, represents the ratio of thermocapillary to capillary forces; the amount of free-surface deformation is proportional to the capillary number. Obviously, the capillary number increases as ΔT is enlarged. The stress acting on the free surface is decomposed into normal and tangential components in order to explain the free-surface distortion and the resultant velocity on it. The net normal stress σ_n increases as $x \to 0$ (Fig. 7(b)), because the static pressure is large there. When ΔT increases, the difference between normal stresses at the stagnation point and contact line is increased, resulting in a stronger pinching effect at the stagnation point than that at the contact line leading to greater apparent deformation.

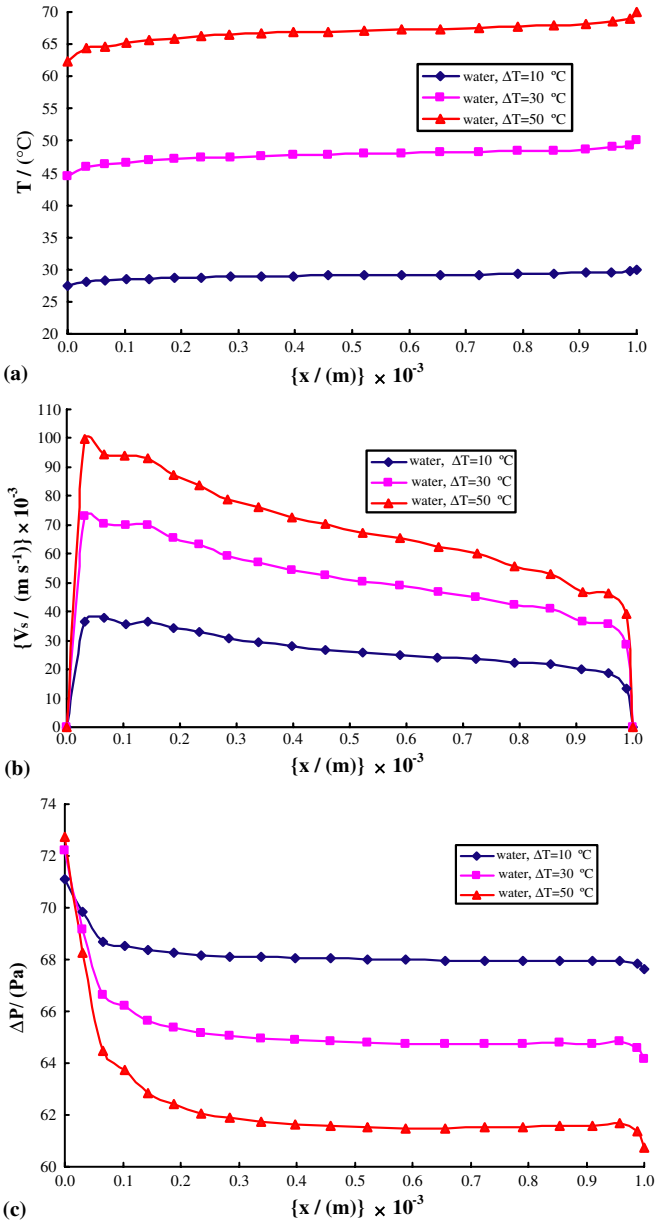

Fig. 5. (a) Temperature, (b) resultant velocity, (c) pressure difference versus x, for a water drop with $D = 1.01 \times 10^{-3}$ m and three different ΔT.

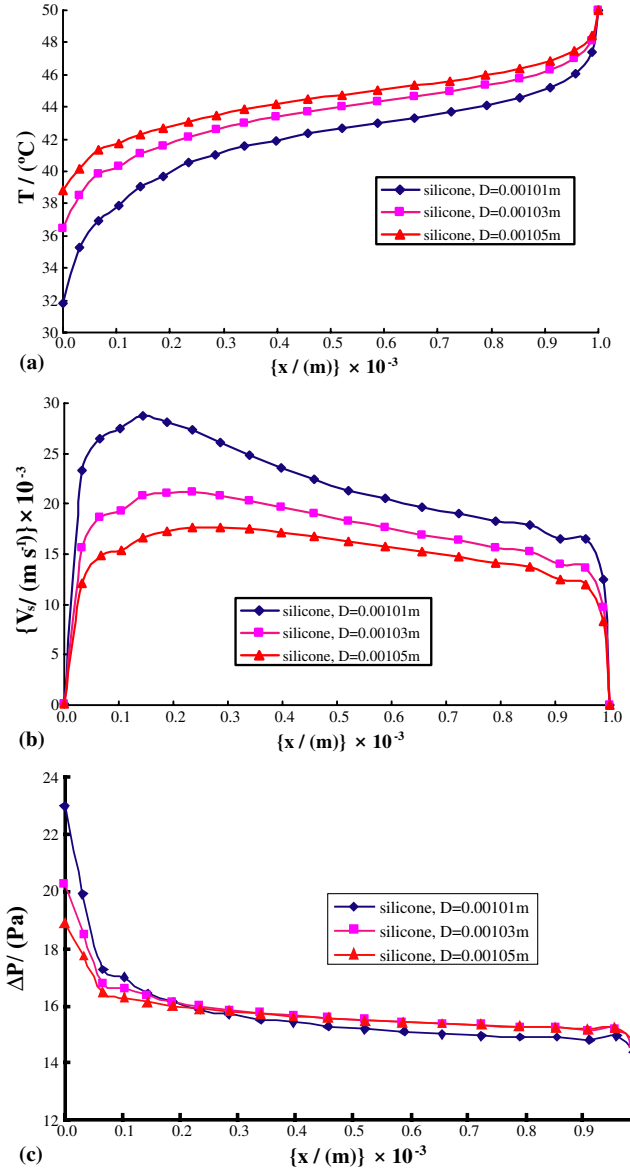

Fig. 6. (a) Temperature, (b) resultant velocity, (c) pressure difference versus x, for a silicone-oil drop with $\Delta T = 30$ °C and three different D.

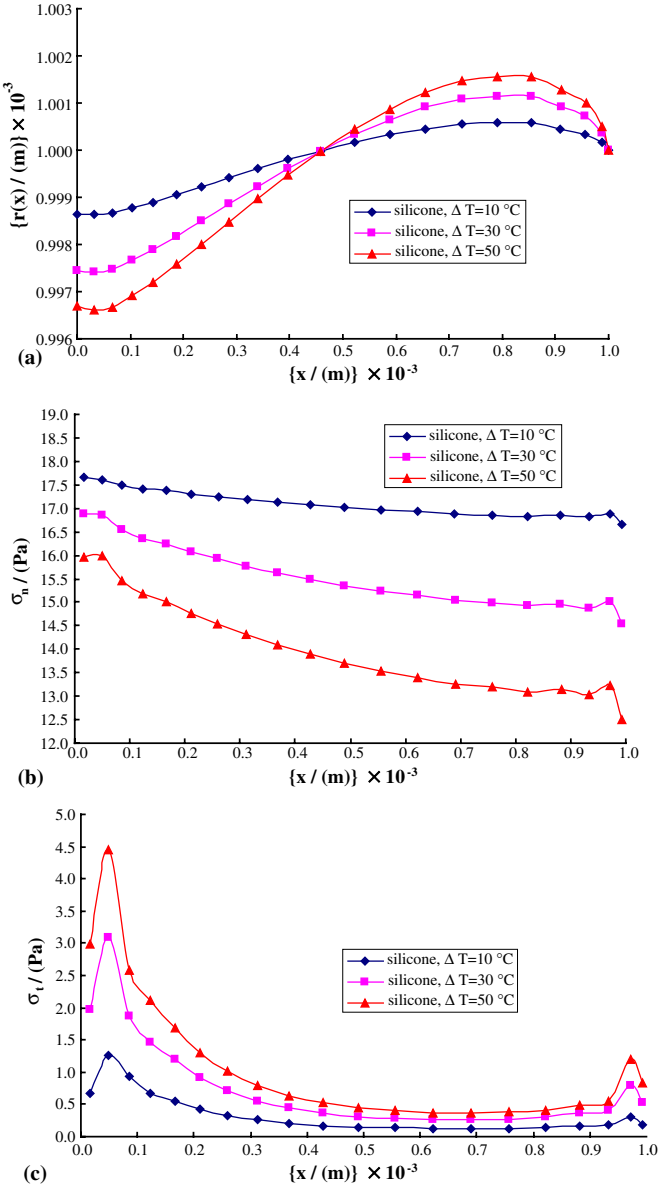

Fig. 7. (a) Drop radius, (b) net normal stress, (c) net tangential stress versus x, for a silicone-oil drop with $D = 1.01 \times 10^{-3}$ m and three different ΔT.

Therefore, the free surface becomes concave inward at the stagnation point, and the drop is convex outward away from the vertex, as required for volume conservation. The net tangential stress $\boldsymbol{\sigma}_t$ decreases as x increases except when $x \to 1$ (Fig. 7(c)), which explains the trends of the velocity curves (Fig. 4(b)). The trends for water droplets are similar to those for silicone oil.

Fig. 8 shows the $S(0)$ of silicone-oil and water as a function of ΔT for $D = 1.01 \times 10^{-3}$ m. Both silicone-oil and water have a vertex height $S(0)$ that decreases, indicating deepening of the dimple, as ΔT increases. The deeper dimple exhibited by the droplet implies a greater pressure at the center, caused by the increased speed of the free-surface, which drags more gas into the interstitial space. Thus, the nonwetting phenomenon can be enhanced by increasing the temperature difference between the hot and cold walls.

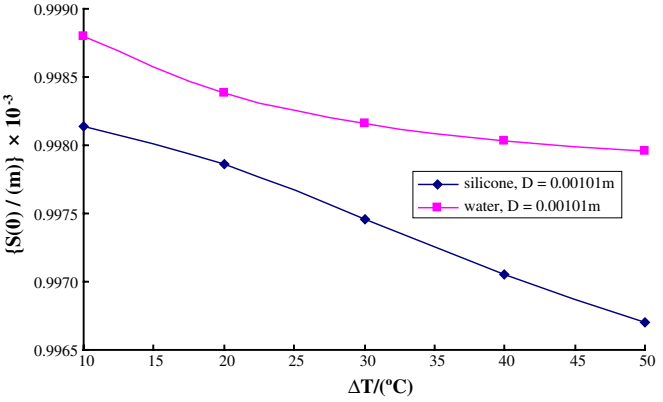

Fig. 8. $S(0)$ of silicone-oil and water drops versus ΔT with $D = 1.01 \times 10^{-3}$ m.

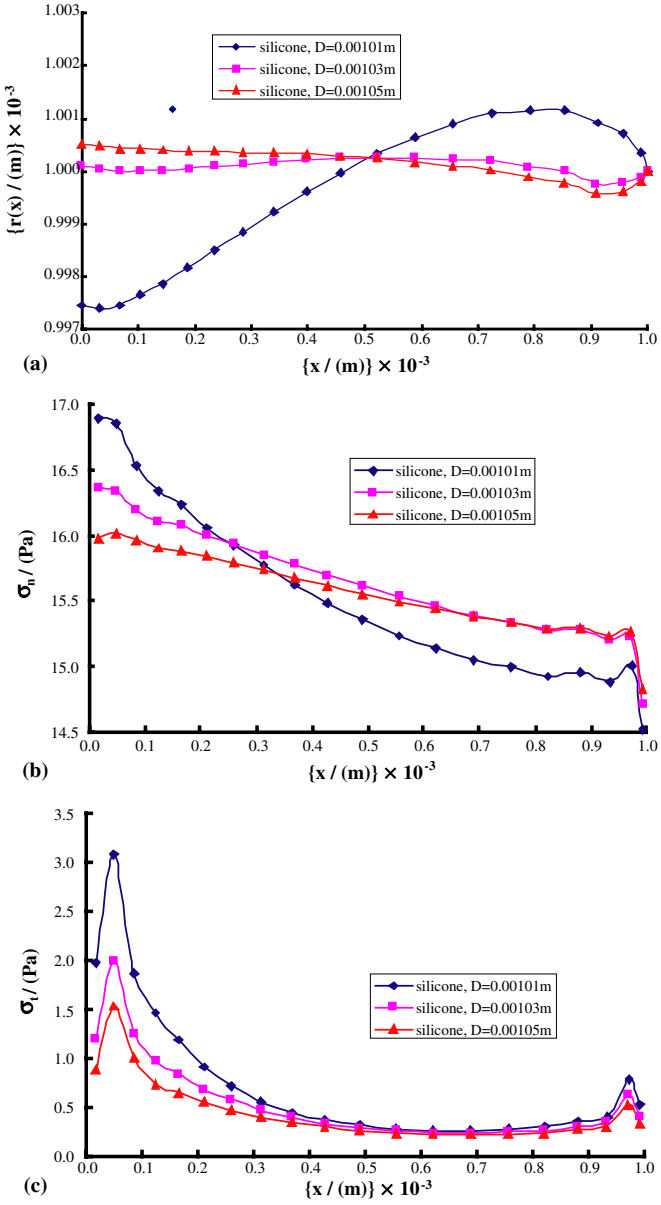

Fig. 9. (a) Drop radius, (b) net normal stress, (c) net tangential stress versus x, for a silicone-oil drop with $\Delta T = 30$ °C and three different D values.

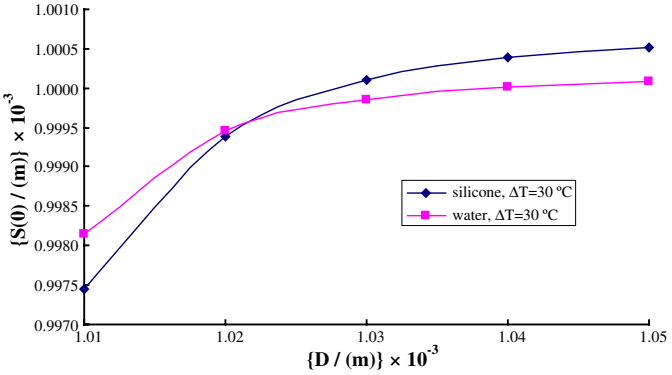

Fig. 10. $S(0)$ of silicone-oil and water drop versus D with $\Delta T = 30$ °C.

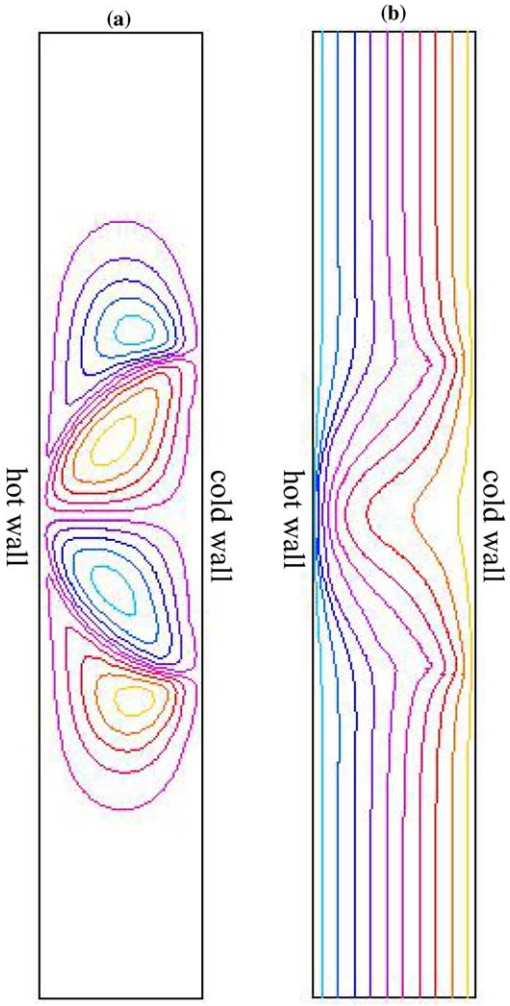

Fig. 11. (a) Streamline contours and (b) isotherms for a cold, silicone-oil drop ($T = 20$ °C) pressed against a hot wall ($T = 35$ °C) and $D = 1.01 \times 10^{-3}$ m.

The experiments reported on in [1–3] were concerned with the axisymmetric analog of the 2-D problem treated here, so a direct quantitative comparison is not possible; the 2-D experiments of Nalevanko [10] do not provide data of sufficient detail to support a quantitative comparison. For $\Delta T = 30$ °C with $D = 1.01 \times 10^{-3}$ m, the capillary number of silicone oil ($Ca_s = 0.1077$) is larger than that of water ($Ca_w = 0.066$). Therefore, the nonwetting effect for silicone is more significant.

The wall distance D influences the free-surface deformation of the silicone-oil drop, as shown in Fig. 9(a), for a fixed $\Delta T = 30$ °C. There is an increased surface-temperature gradient for a smaller D, because the thermal resistance of the lubricating film decreases. Therefore, $r(0)$ (=$S(0)$) decreases as D decreases. The net normal stress increases with decreasing D as $x \to 0$ (Fig. 9(b)), exhibiting the opposite trend away from the apex approaching the contact line. For $D = 1.01 \times 10^{-3}$ m, the free surface dimples at the stagnation point and bulges nearer the contact

line. The net tangential stress increases as D is decreased (Fig. 9(c)). The trends for the water drop are similar to those of silicone oil.

Fig. 10 shows $S(0)$ for silicone-oil and water droplets as a function of wall distance D for $\Delta T = 30\ ^\circ\mathrm{C}$. $S(0)$ decreases (i.e., indicating increased dimpling) with decreasing D for both silicone oil and water. The dimpling for water appears to be less than that for silicone oil for $D < 1.02 \times 10^{-3}$ m.

The simulation may also be used to investigate the case in which a *cold* droplet is moved toward a hot wall. The thermal boundary conditions of the two solid surfaces are now reversed. The streamline contours and isotherms for silicone oil are plotted in Fig. 11 for an upper-wall temperature of $T = 35\ ^\circ\mathrm{C}$ and a lower-wall temperature of $T = 20\ ^\circ\mathrm{C}$. A pair of symmetric, counter-rotating vortices also appear within the droplet (Fig. 11(a)), but the direction of rotation is opposite to that observed in Fig. 3(a). The shapes of the isotherms shown in Fig. 11(b) are unlike those in Fig. 3(b), due to the opposite flow direction. The lubricating film near the upper, hot wall flows from infinity toward the symmetry axis, and is then dragged along the silicone-oil free surface.

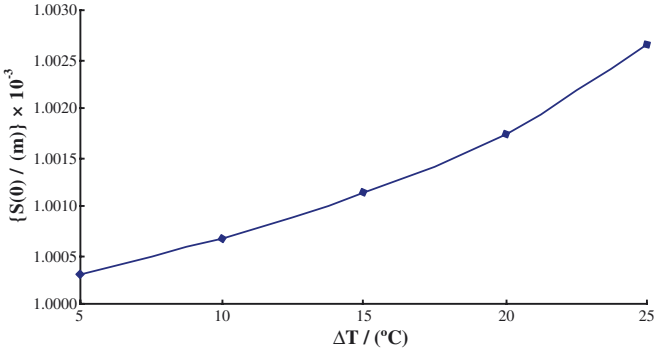

Fig. 13. $S(0)$ of silicone-oil versus ΔT for the conditions of Fig. 11.

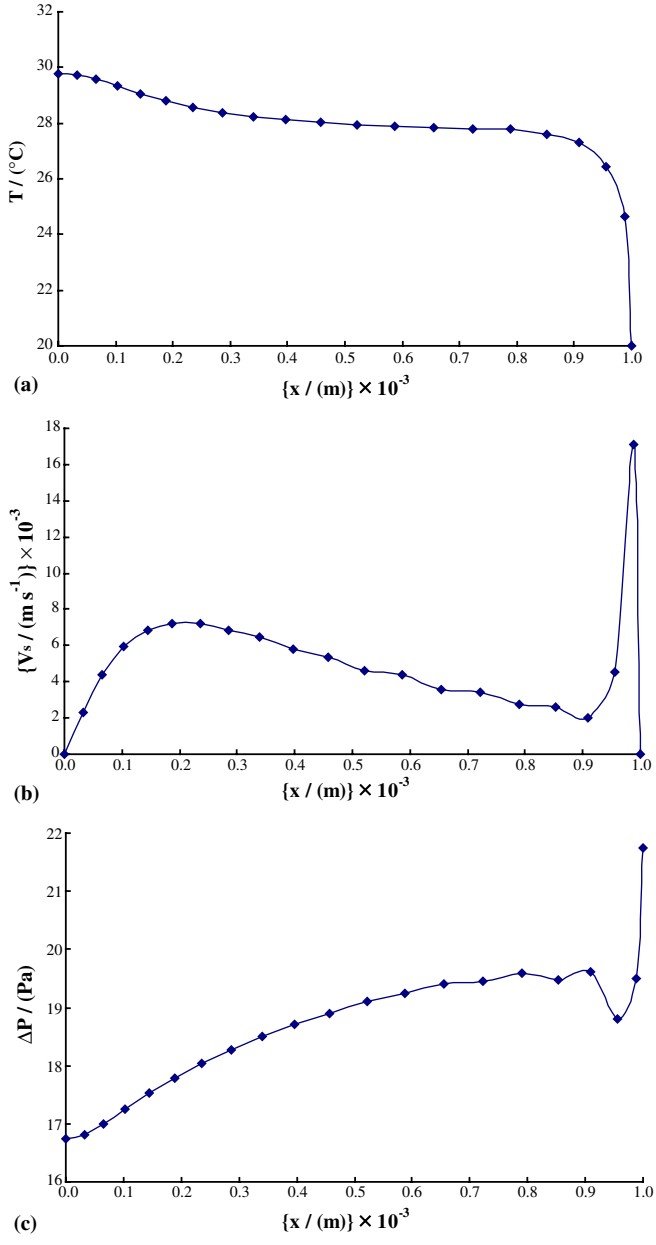

Fig. 12. (a) Temperature, (b) resultant velocity, (c) pressure difference versus x for the conditions of Fig. 11.

Fig. 12 shows surface temperature, speed and pressure differences for this situation. The surface temperature decreases slowly when x increases, decreasing abruptly near $x = 1$ (Fig. 12(a)). The droplet free surface has an intense temperature gradient near the cold wall ($x = 1$) to which is pinned. Hence, the silicone oil appears to have a higher velocity here (Fig. 12(b)). The velocity gradients near $x = 0$ are much smaller than those near $x = 1$. Contrary to the results for the hot droplet case shown in Fig. 5(c), the pressure difference on the free surface at $x = 0$ decreases as the droplet is moved closer to the hot wall (Fig. 12(c)). In this scenario, the thermocapillary motion of the free surface actually serves to drain the lubricating gas from the space between the liquid free-surface and the hot wall, tending to promote, rather than prevent, wetting. Fig. 13 shows the height at the drop vertex for a 5 cSt silicone-oil drop, showing that the greater the temperature difference, the larger the vertex bulge.

4. Conclusion

In this paper, the thermocapillary nonwetting effect has been modeled by employing finite-element numerical simulations performed with the commercial code FIDAP, to study the individual effects of ΔT and D on the stagnation point displacement for semicircular drops of silicone-oil and water.

For a heated drop approaching a cold wall, air driven by thermocapillary-induced free-surface motion is swept into the space between the droplet and cold wall to continuously replenish the lubricant, promoting the maintenance of a nonwetting state. This air-flow magnitude, and hence,

the nonwetting, may be increased by increasing either ΔT or decreasing D. A silicone-oil droplet subjected to the same conditions has a larger capillary number than that of water. Therefore, a silicone oil drop more easily exhibits deformation when D is small enough. Finally, it is observed that wetting is enhanced rather than inhibited when a cold drop is pressed against a hot plate, for gas is drained away from the lubricating film.

Acknowledgement

GPN was supported by a grant from the Office of Biological and Physical Research of NASA.

References

[1] P. Dell'Aversana, J.R. Banavar, J. Koplik, Suppression of coalescence by shear and temperature gradients, Phys. Fluids 8 (1996) 15–28.
[2] P. Dell'Aversana, V. Tontodonato, L. Carotenuto, Suppression of coalescence and of wetting: the shape of the interstitial film, Phys. Fluids 9 (1997) 2475–2485.
[3] P. Dell'Aversana, G.P. Neitzel, Behavior of noncoalescing and nonwetting drops in stable and marginally stable states, Exp. Fluids 36 (2004) 299–308.
[4] P. Dell'Aversana, G.P. Neitzel, When liquids stay dry, Phys. Today 51 (1998) 38–41.
[5] G.P. Neitzel, P. Dell'Aversana, Noncoalescence and nonwetting behavior of liquids, Annu. Rev. Fluid Mech. 34 (2002) 267–289.
[6] L.B.S. Sumner, A.M. Wood, G.P. Neitzel, Lubrication analysis of thermocapillary-induced nonwetting, Phys. Fluids 15 (2003) 2923–2932.
[7] R. Monti, R. Savino, Correlation between experimental results and numerical solutions of the Navier–Stokes problem for noncoalescing liquid drops with Marangoni effects, Phys. Fluids 9 (1997) 260–262.
[8] R. Monti, R. Savino, S. Tempesta, Wetting prevention by thermal Marangoni effect. Experimental and numerical results, Eur. J. Mech. B 17 (1998) 51–77.
[9] L.B.S. Sumner, G.P. Neitzel, J.-P. Fontaine, P. Dell'Aversana, Oscillatory thermocapillary convection in liquid bridges with highly deformed free surfaces: experiments and energy-stability analysis, Phys. Fluids 13 (2001) 107–120.
[10] J. Nalevanko, Design of an apparatus for investigation of 2-D liquid drop non-coalescence, M.S. Thesis, Georgia Institute of Technology, 1997.
[11] B.M. Carpenter, G.M. Homsy, Combined buoyant-thermocapillary flow in a cavity, J. Fluid Mech. 207 (1989) 121–132.
[12] S. Ostrach, Low-gravity fluid flows, Annu. Rev. Fluid Mech. 14 (1982) 313–345.
[13] C.-W. Kuo, J.-C. Chen, G.P. Neitzel, Numerical simulation of isothermal nonwetting, Int. J. Numer. Meth. Fluids, in press.
[14] M.K. Smith, G.P. Neitzel, Multiscale modeling in the numerical computation of isothermal non-wetting, J. Fluid Mech. 554 (2006) 67–83.